THE INFLUENCE OF SPUTTER GAS PRESSURE ON THE HARDNESS AND MODULUS OF TANTALUM THIN FILMS

A Thesis

Presented to the Faculty of the Graduate School

of Cornell University

In Partial Fulfillment of the Requirements for the Degree of

Master of Science

by

Shangchen Han

August 2013

ABSTRACT

Sputter deposited tantalum (Ta) thin films can form in 2 phases: the metastable tetragonal phase (β-Ta) and the bulk bcc phase (α-Ta), both of which have wide applications. Producing Ta films with desired structure and properties is important, e.g. Ta films used for x-ray masks are required to have low stress; diffusion barriers between Cu and Si for semiconductors prefer α-Ta over β-Ta. Varying sputter pressure while keeping other sputter parameters constant can be an effective way to tune both structure and properties of Ta films. It has been shown that, under good control of sputter parameters, we can get consistent variations in structure (stress, grain size) in β-Ta films with increasing Ar gas pressure. This thesis shows that stress has little effect on β-Ta indentation properties while variations in hardness can be well explained by the variation in grain size. All the metastable β-Ta films transformed into α-Ta after thermally cycled to 700^{o} C. Nanoindentation results showed that both the hardness and indentation modulus are affected by the unique film structure of α-Ta films, which is characterized as having continuous orientation gradients and discontinuous grain boundary structure.

BIOGRAPHICAL SKETCH

Shangchen Han was born in Qiqihaer, Heilongjiang Province in China. His family moved to Shanghai, one of the biggest cities in China, at the age of 12 and started a new life after that. He graduated from Zhejiang University with a bachelor's degree in Materials Science and Engineering. To get more research experience, he decided to come to the Materials Science and Engineering Department at Cornell University. Life in Ithaca was peaceful and interesting for him. Academic study in Cornell has made him more open-minded as well as more equipped for future career. Upon completing his degree, Shangchen is looking forward to going to the West Coast of the United States to explore more academic opportunities.

ACKNOWLEDGMENTS

A lot of people have made my past two years in Cornell University inspiring and enjoyable. First and foremost, I want to thank my advisor, Shefford Baker. I was impressed by his academic preciseness, strong communication ability in life and extensive knowledge in different aspects in the academic world. I appreciate his dedication to my project in both theory and experimentation. His attitude "we want to be right" towards research not only make me realize how to do great research work, but also how to make contributions to any area in real world. I would also like to thank my second committee member, Eve Donnelly, for her advice and support. She is a great advisor in research as well as a great teacher in class.

I want to thank the members of the Baker research group for all their help throughout my time at Cornell. Thanks to Markus Chmielus and Elizabeth Ellis for all their work in the tantalum thin film projects. In those group projects, I've learned a lot from them in analyzing data and interpreting literature. Markus is currently looking for a faculty job and I'm sure with his talent and passion, he will become an excellent professor in the future. Elizabeth has been dedicated to anything she worked at. Her career is about to get remarkable soon. I also thank the nanoindentation group members, Jayme Burket, Miki Kunitake, Lisa Lamberson and Joe Carloni, for their help in nanoindentation experiments. They provided a lot of suggestions in collecting reliable data.

Without my friends, my life would have been monotonous. My conversation partner, Tim Cowley, a postdoc in Cornell, patiently led me into understanding the culture and environment in the United States. I thank all my neighbors who have made my life colorful. This is the best apartment I've ever lived in. I thank all my friends that cares about me.

Finally, I want to thank my family, especially my parents, for their support for my every decision. Life became much easier when I know there are people who always love me unconditionally.

TABLE OF CONTENTS

Chapter 1

Introduction

1.1 Motivation

Thin film usually refers to the thin layer attached to a substrate where the substrate is much thicker than the layer. They have been widely used throughout the world in recent years. Thin films can have very different properties from their bulk counterparts due to their large surface-to-volume ratio, reduced dimensions and constraints caused by the substrates. While these materials are often chosen on the basis of their electronic, magnetic, or optical properties, understanding their microstructures and mechanical properties is also important in their applications.

Sputter deposited tantalum (Ta) thin films have been found to form in 2 phases: a tetragonal phase (β-Ta) and a bcc phase (α-Ta), both of which have wide applications. However, producing Ta films with desired structures and properties has been challenging. It has been shown that under good control of sputter parameters, we can get consistent variations in structure in both as-deposited β-Ta and phase transformed α-Ta films with increasing Ar gas pressure. The focus of this thesis is to understand how changes in the microstructure induced by changes in the working gas pressure during sputter deposition affect nanoindentation hardness and modulus of β-Ta and phase-transformed α-Ta thin films.

1.2 Structure of this thesis

This thesis consists of five chapters. Chapter 1 is the background information of Ta thin films and an overview of the nanoindentation method. Chapter 2 introduces experimental techniques used in chapter 3 and 4. Chapter 3 is a draft of a paper entitled "The influence of sputter gas pressure on the structure and properties of high purity β-tantalum thin films" in which my primary contribution is the nanoindentation tests. Chapter 4 shows the nanoindentation properties of the phase transformed α-Ta films. Finally, Chapter 5 provides the conclusions of the whole thesis and suggests future work to further understand Ta thin films.

1.3 Tantalum thin films

The atomic number of Ta is 73. Bulk Ta has a bcc structure, a resistivity at room temperature of 13.6 μΩ cm [1], temperature coefficient of resistance of +3800 p.p.m./℃ [2], a high melting temperature (3292 K) [3], and high resistance to chemical attack [4]. More than 70% of tantalum is consumed by the electronics industry, and most of that goes into making capacitors [5].

Ta thin films can be sputter deposited in 2 phases: α-Ta and β-Ta. α-Ta has a bcc structure, the same as bulk Ta. It can be used for corrosion- and wear-resistant coatings due to its refractory nature and high ductility [6] and the diffusion barrier between copper and silicon [7]. β-Ta is a metastable phase which was only found in thin films. It has a

complex tetragonal structure [8,9], with a resistivity of 180-220 μΩ cm [1], a coefficient of resistance of -150 p.p.m./℃. It has been widely used as thin film resistors [10] and x-ray masks [11,12].

A lot of efforts have been made to understand how the sputter conditions can affect Ta film structure and properties. Several factors have been identified: substrate temperature [13], sputter pressure [14–16], film thickness [17], substrate used for deposition [18], substrate bias voltage [19], adhesion layer between substrate and film [20], impurity incorporation [21] etc. Besides depositing films directly, phase transformation from the metastable β-Ta to α-Ta is another approach to producing tantalum thin films [22]. This section will focus on sputter deposition of tantalum thin films as well as phase transformed α-Ta produced by thermal cycling.

1.3.1 Phases in sputter-deposited Ta films

β-Ta was first identified by Read and Altman [1] in 1965. A tetragonal unit cell containing 16 atoms was suggested at first based on the x-ray diffraction pattern. In 1972, Moseley and Seabrook [8] suggested a unit cell containing 30 atoms with a=10.194, c=5.313. The crystal symmetry was identified to be $P4_2/mnm$ space group, isomorphous with β-uranium. The calculated density was 16.33 g/cm^3. ICDD (International Centre for Diffraction Data) database then replaced Read's cell with Moseley's cell [23]. In 2002, Arakcheeva et al. [9] successfully obtained small single crystals of β-Ta from molten fluorides. Based on single crystal X-ray diffraction data, they proposed a σ type Frank–

Kasper structure with crystal symmetry of $P\bar{4}2_1m$ space group [9,24]. In comparison, $P4_2/mnm$ space group allows only even (00*l*), but not odd (00*l*) reflections while $P\bar{4}2_1m$ allows both even and odd (00*l*) reflections. Based on the appearance of odd (00*l*) reflections, Lee et al. [23] and Jiang et al. [25] have suggested that $P\bar{4}2_1m$ is the right structure. Jiang et al. analyzed the differences between a $P4_2/mnm$ structure and a $P\bar{4}2_1m$ structure (depicted in Figure 1.1): (1) both structures consist of two antisymmetrically superposed pseudohexagon layers as the primary nets (denoted as B and C), but atoms comprising the B and C layers in the $P\bar{4}2_1m$ structure slightly deviate from a planar structure; (2) the atoms in the two neighboring interlayers (denoted as A) have the same coordinates in the $P4_2/mnm$ structure but different coordinates in the $P\bar{4}2_1m$ structure. Therefore $P\bar{4}2_1m$ has an $A_1BA_2CA_1BA_2C$... stacking order while $P4_2/mnm$ has an ABACABAC... stacking order.

Substrates used for deposition is one factor that affects the phase present in a Ta film. Feinstein et al. [18] suggested that O or OH needs to be present at the nucleation surface for the formation of β-Ta. They also suggested that which of the two phases is formed is determined at the nucleation phase. This finding was later modified by Sato [26], who observed that substrates with high resistance to oxidation tend to nucleate α-Ta, while substrates with low resistance to oxidation tend to nucleate β-Ta. Some studies have been particularly contributed to depositing α-Ta films. Growing a thin layer (Ti, Cr, MgO etc.) between the substrate and film [20,27,28], pre-treatment of the substrate (e.g. Ar/N_2 plasma pre-treatment [29]) and heating the substrate during deposition above 600 ℃ [13]

have been proven to be effective in depositing α-Ta.

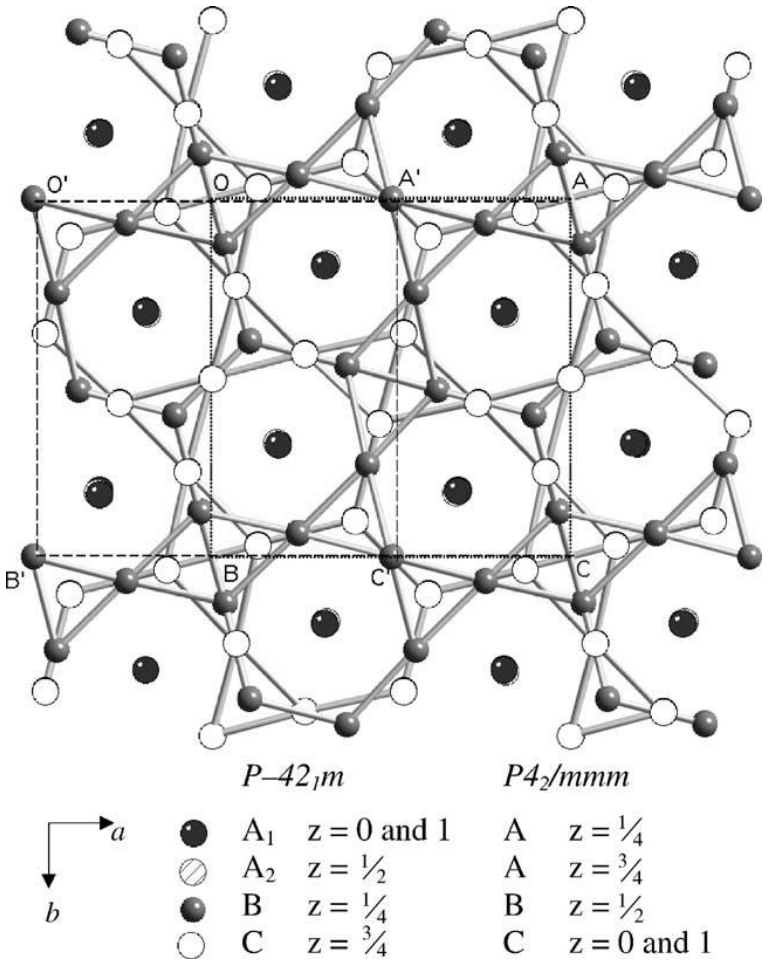

Figure 1.1: Structures of the $P\bar{4}2_1m$ and the $P4_2/mnm$ space groups. AOBC and A'O'B'C' indicate the unit cells of $P4_2/mnm$ and $P\bar{4}2_1m$ space groups, respectively [25].

The influence of impurities (i.e. Ar, O, H, N) incorporated during the sputter process in tantalum thin films might result in α- or β-Ta and is inconclusive with different labs receiving opposite phases [30]. Read and Altman [1] said that β-Ta is as pure as or purer than α-Ta when they first identified this phase. Schwartz [31] claimed β-Ta is the

impurity-free phase and α-Ta will form when controlled amounts of impurities are added. But Westwood [32] said β-Ta is an impurity phase formed to accommodate impurities above the solubility limit of α-Ta. Croset and Velasco [33], on the other hand, proposed that impurities do not influence the growth of either phase, but that low sputter power and low substrate temperature favor the formation of β-Ta. It was concluded by Baker [30] that while impurities seem to have an influence on the formed Ta phase, too many changing parameters from experimental run to run and sputter system to sputter system also influence Ta phase formation.

1.3.2 The influence of sputter gas pressure on as-deposited Ta films

Thin films on substrates are constrained to adopt the in-plane dimensions of the substrate and large stresses arise. The changes in the equilibrium in-plane dimensions of the film relative to those of the substrate lead to stresses in the films. This stress is the film-substrate interaction stress and is referred to as stress for short in this thesis. It was shown that different sputter pressure results in different as-deposited stress in thin films [34,35]. Clevenger et al. [16] deposited β-Ta films with Ar pressure ranging from 1.6 to 150 mTorr and found the as-deposited film stress increased monotonically from large compressive stress (-2.2 GPa) to large tensile stress (1.2 GPa) with increasing sputter pressure (Figure 1.2). They explained this phenomenon by the effect of energetic ions and atoms on the as-deposited film microstructure. Loosely packed columnar grains with low density grain boundaries deposited at high Ar pressure could account for the tensile stress

while an increasingly energetic ion and atom bombardment at lower deposition pressures could drive more atoms into grain interior and result in compressive stress.

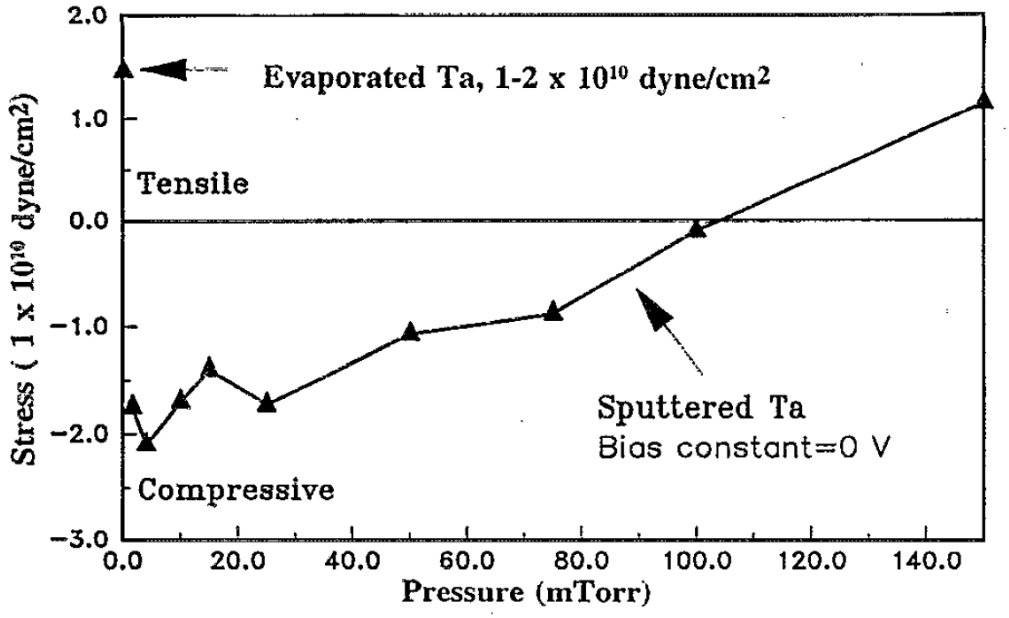

Figure 1.2: Stresses of β-Ta films deposited at Ar pressure from 1.6 to 150 mTorr. Large compressive stresses formed at low sputter pressures and then transitioned to large tensile stresses at high Ar pressures [16].

Thornton [36] proposed that sputter pressure dependent stress results from collisions between the sputtered atoms and Ar atoms. The number of collisions is usually related to the pressure-dependent mean free path [37]:

$$\lambda = \frac{kT}{\sqrt{2}\pi d^2 p}$$

where k is the Boltzmann constant (1.38×10^{-23} J/K), T is the temperature, d is the diameter

of the sputtered atom, p is the sputter pressure. When the mean free path of the sputtered atom is larger than the target–substrate distance L, sputtered atoms will reach the substrate without collisions. The more energetic atoms will penetrate the film due to an atomic peening effect. They are more likely to reach their equilibrium positions or even become interstitial atoms and high compressive stresses arise. When $\lambda < L$, the atoms will be less energetic and may produce a porous structure [38]. Windischmann [39] suggested that at high energies of incoming species, atomic peening causes compressive stress which transitions to tensile stress where grain boundary zipping with increasing sputter pressure could happen.

Besides stress change, other factors have also been found to be affected by Ar pressure. In a paper by Oda et al. [12], the concentration of Ar in the films was decreasing with increasing sputter pressure. It is not clear if sputter pressure affects the phase present in the Ta films. On Si (100) wafers, Clevenger et al. [16] got β-Ta under Ar pressures from 1.6 to 150 mTorr. On the same substrate, Javed et al. [40] got α-Ta below 6.5 mTorr Ar pressure and β-Ta at 7 mTorr Ar pressure. Navid and Hodge [15] got α-Ta at Ar pressures of 0.5 and 0.7 Pa and either mixed phases of β-Ta and α-Ta or pure β-Ta at the other Ar pressures (between 0.3 and 1.4 Pa). They indicated that their studies are typically not reproducible and depend on many parameters which can change from sputter system to sputter system.

1.3.3 Structure evolution in thermal cycling

The phase transformation from β-Ta to α-Ta occurs during a thermal cycling process [16,22,41]. The stress vs. temperature plots corresponding to β-Ta films on Si (100) substrate and fused silica are shown in Figure 1.3 [22]. Each film was thermally cycled to 600 ℃ after deposition. Due to different thermal expansion coefficient (CTE) and biaxial modulus between Ta and the substrate, a change in temperature resulted in significant stress change in thin films. Based on the slope of the heating and cooling curves for Ta films on Si (100) and fused silica substrates, Knepper [22] determined the CTE and biaxial modulus for both β-Ta and α-Ta (Table 1.1). Between 300 ℃ and 400 ℃ for the film on Si (100) and 250 ℃ and 400 ℃ for the film on fused silica, there was a large stress increase for both films corresponding to the phase transformation from metastable β-Ta to α-Ta.

Table 1.1: CTE and biaxial modulus of β-Ta and α-Ta films compared with bulk α-Ta [22]

	β phase	α phase	bulk α phase
Average CTE ($\times 10^{-6}$ /° C)	6.0 ± 0.8	6.9 ± 0.9	6.5
Average Biaxial Elastic Modulus (GPa)	170 ± 20	265 ± 30	230 [(100) orientation] 310 [(111) orientation]

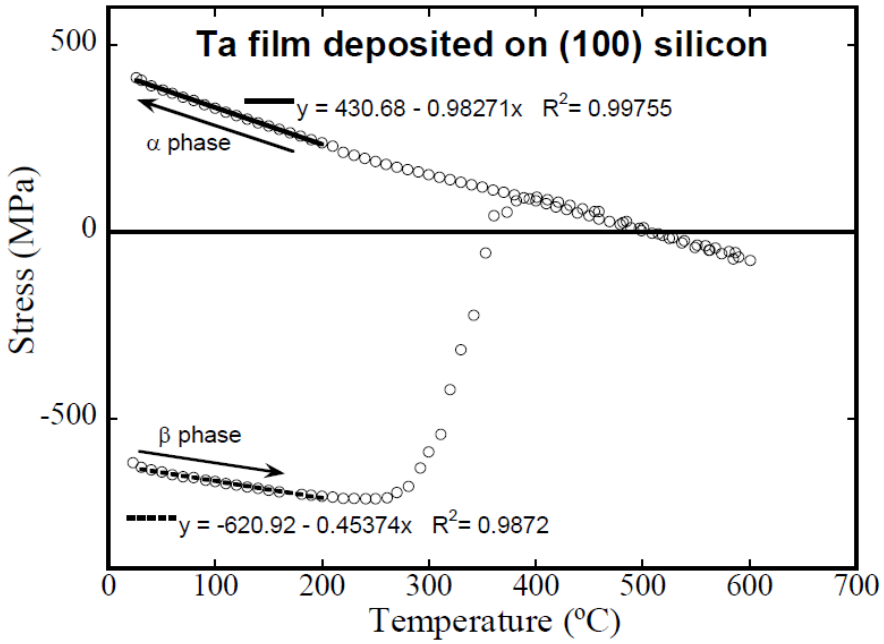

(a)

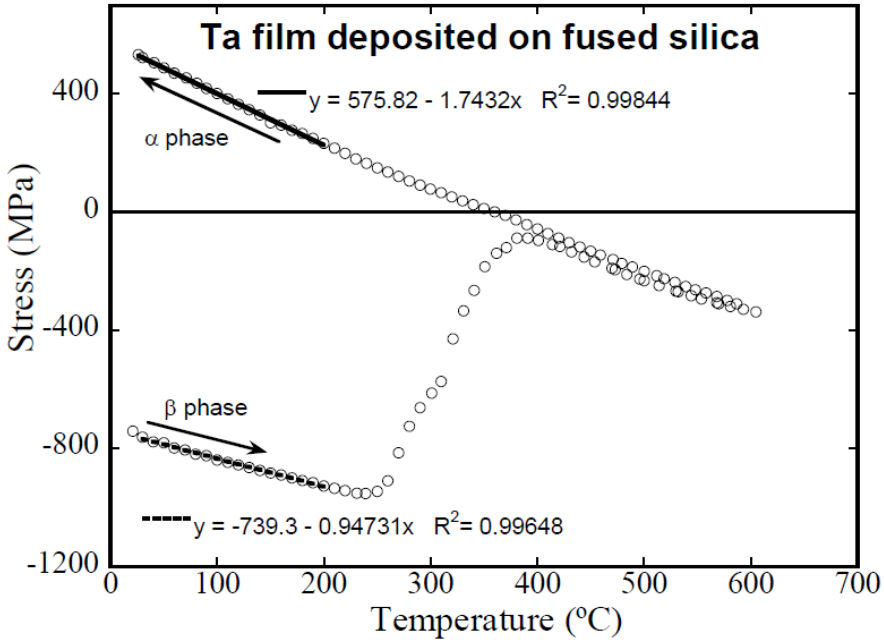

(b)

Figure 1.3: Stress vs. temperature data for as-deposited β-Ta on a (a) ~ 0.5 mm Si (100) substrate and (b) ~ 0.5 mm fused silica substrate [22].

The threshold temperature of phase transformation has been found to be as low as 250 ℃ [22] and as high as up to 800 ℃ [42]. This enormous discrepancy could result from the influence of the annealing atmosphere as small amounts of oxygen could inhibit the phase transformation [22]. After the phase transformation, an unusual structure formed (Figure 1.4) [22]. The phase-transformed α-Ta films have a discontinuous grain boundary structure and consistent gradients in crystal orientation within individual grains of up to 4 ⁰μm over a distance of several micrometers. This structure was suggested to be accommodated by aligned arrays of edge dislocations on primary slip systems parallel or nearly parallel to the plane of the film. The grain boundary spacing was found to be ~2 μm which is much bigger than the as-deposited β-Ta grain size.

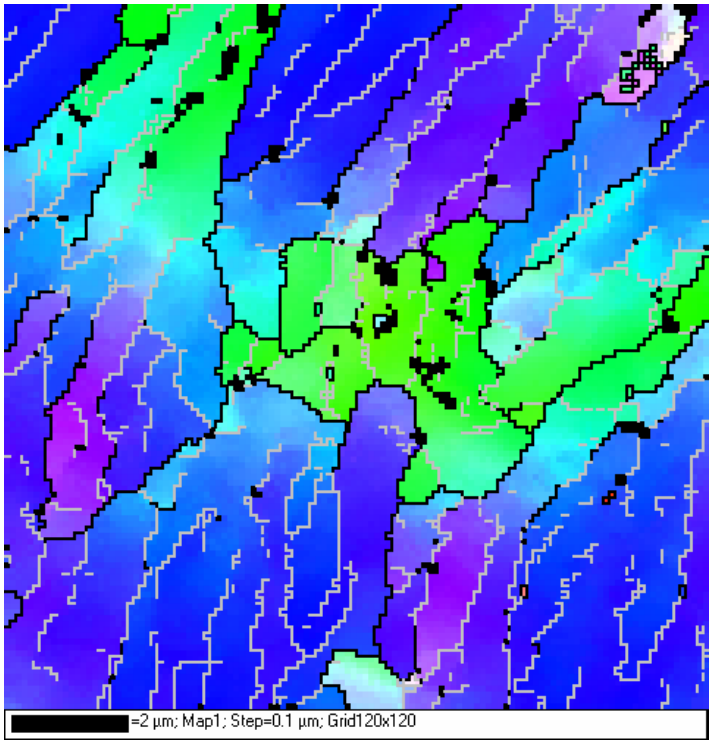

Figure 1.4: An EBSD graph of a phase transformed α-Ta film [22].

1.4 Nanoindentation tests on thin films

Nanoindentation is a depth sensing method which records the load-displacement curve during indentation. Compared with traditional hardness tests, this method excludes the necessity to image small indentations to extract the hardness while enabling us to extract the elastic properties of the materials apart from hardness. This chapter reviews the nanoindentation model as well as factors that affect nanoindentation data in thin films.

1.4.1 Nanoindentation model

The most widely used nanoindentation model was proposed by Oliver and Pharr [43] in 1992. The basis of this model is an elastic contact model derived by Sneddon [44] in 1965. His results showed that the load-displacement relationships for many simple indenter geometries can conveniently be described as a power-law relationship:

$$P = \alpha h^m$$

where P is the load of the indenter, h is the displacement of the indenter, α is a material related constant and m is an indenter geometry related constant. In 1992, based on this relationship, Oliver and Pharr [43] demonstrated a comprehensive technique that applies to any axisymmetric indenters with any infinitely smooth profile. Figure 1.5 shows a load-displacement curve of an indentation test. The initial unloading stiffness was represented as:

$$S = \frac{dP}{dh} = \beta \frac{2}{\sqrt{\pi}} E_r \sqrt{A}$$

where β is an indenter shape dependent constant which is usually denoted as 1.034 for a Berkovich tip, A is the projected contact area at maximum load and E_r is the reduced modulus related to the elastic moduli (E) and Poisson's ratios (v) of both the indenter and the indented material:

$$\frac{1}{E_r} = \frac{1-v^2}{E} + \frac{1-v_i{}^2}{E_i}$$

in which $\frac{1-v^2}{E}$ can be considered as the material specific modulus [45]. The nanoindentation hardness is then given by:

$$H = \frac{P_{max}}{A}$$

where P_{max} is the maximum load in Figure 1.5.

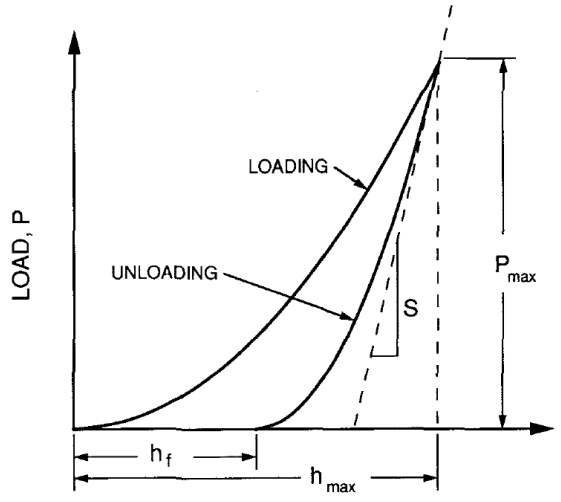

Figure 1.5: A typical load-displacement curve of a nanoindentation test [43].

The contact profile in Figure 1.6 has to be considered to determine the contact depth which is used to extract the contact area through an area function (introduced in Chapter

2). Based on Sneddon's solution, the elastic displacement at maximum load is given by:

$$h_s = \varepsilon \frac{P_{max}}{S}$$

where ε is an indenter geometry related constant: ε = 0.72 for a conical tip and ε = 0.75 for a Berkovich tip. The contact depth is then given by:

$$h_c = h - h_s$$

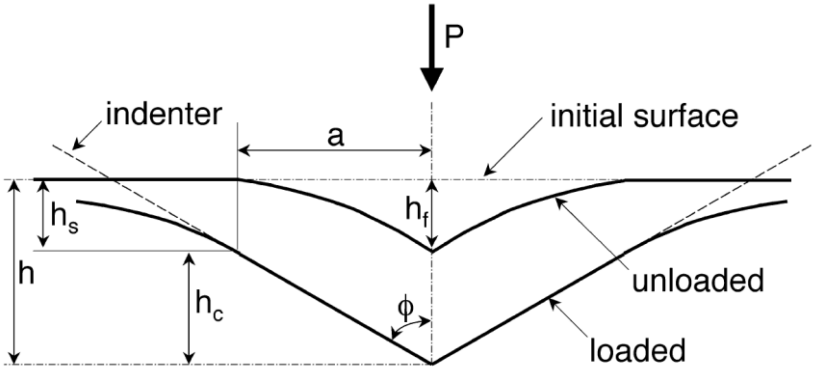

Figure 1.6: A schematic representation of a section through an indentation test [46].

1.4.2 Factors that affect nanoindentation results in thin films

Although the nanoindentation model has been widely accepted, when we measure the mechanical properties of thin films, it can still give some confusing results due to the geometrical constraint of the substrates, the complicated structures of thin films, etc.

As the indenter approaches the substrate, it is measuring more of the substrate properties rather than the film properties. Saha et al. [47] studied the nanoindentation properties of Al on substrates ranging from soft material (Al) to hard material (Sapphire)

and found that hardness was constant at depths between $0.05 < h/t < 0.2$ where h is the indentation depth and t is the film thickness while modulus was more sensitive to the substrate effect. It was also found that pile-up [48] or sink-in [49] due to the effect of the substrate could happen. These facts made it difficult to establish an efficient numerical model to take the substrate effect into account. The general tactic is making indentations far smaller than the film thickness to avoid substrate effect in nanoindentation tests.

Since stresses in thin films are generally very high, the influence of stress on thin film properties has to be considered in nanoindentation tests. An early work by LaFontaine et al. [50] suggested the apparent yield strength follows a linear relationship with stress: $Y = Y_0 + a\sigma$. As pointed out by Tabor [51], the hardness is related to the uniaxial yield stress Y by: $H = cY$. As a result, hardness also follows a linear relationship with σ by $H = H_0 + b\sigma$. In 1996, Tsui [52] and Bolshakov [53] did both experiments and finite element analysis to analyze the influence of stress on nanoindentation properties. Tsui [52] pointed out that the stress might enhance or decrease indentation plasticity and produce a higher or lower measured hardness. However, it's also possible that the stress around the indenter is altered enough by the plastic flow during indentation that the residual stress exerts no influence on hardness. He observed big differences between contact areas extracted from load-depth curves and from microscope measurements. Using the residual indentation areas measured by microscope, he found residual stress has no influence on hardness and modulus of the material (Figure 1.7). The companion work by Bolshakov [53] confirmed Tsui's observation by finite element simulation that the residual

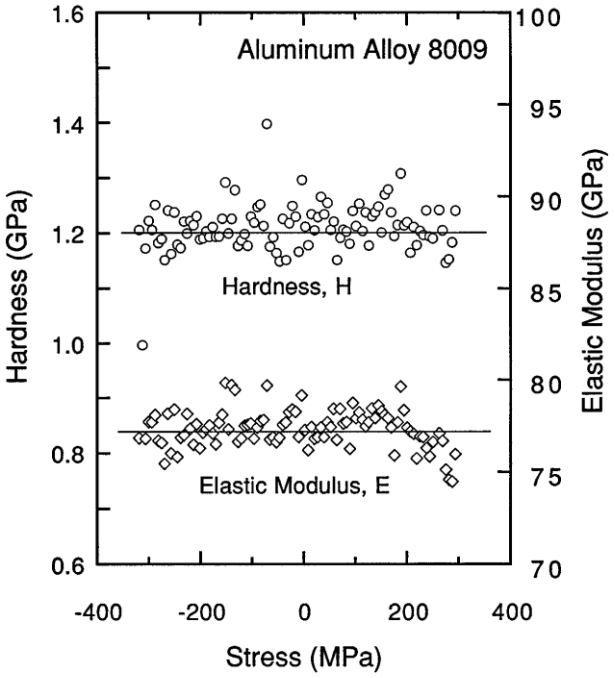

Figure 1.7: Hardness and modulus vs. stress for the aluminum alloy 8009 under uniaxial stress [52].

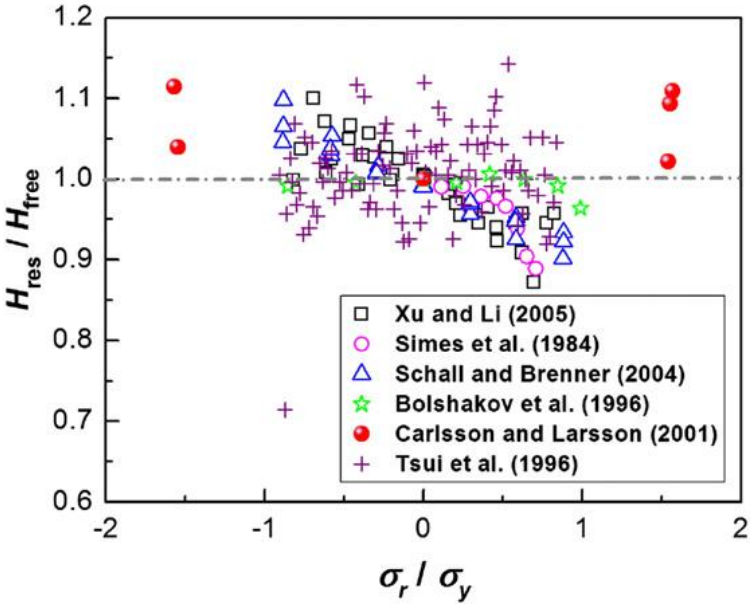

Figure 1.8: Available results of influence of stress on hardness summarized by Ma et al. [54].

stress only influences the pile-up around the indentation region: samples under compression exhibited greater pile-up while samples under tension exhibited smaller pile-up. Since the contact areas extracted from load-depth curves do not take pile-up into account, they could be different from the real contact areas. After the real contact areas were used in the analysis, the hardness and modulus were observed to be independent of the residual stress. These two studies were the basis of several following numerical models [55–58]. Carlsson and Larsson [57,58] studied the effect of residual elastic stress and plastic strain on indentation data and concluded that elastic stress only affects the indentation pile-up while plastic strain increases the yield stress of the material and enhance the hardness of the material. Similar conclusion was also made by Ling et al. [59]. Ma et al. [54] summarized several work (Figure 1.8) and showed that the change of hardness with stress is usually small.

The influence of grain sizes on the mechanical properties has been thoroughly understood. The early studies by Hall [60] and Petch [61] showed:

$$\sigma = \sigma_0 + kd^{-1/2}$$

where σ_0 and k are material constants, d is the grain size and σ is the yield strength of the material. Since hardness can be related to yield strength by $H = C\sigma$, the Hall-Petch relationship can also be written as:

$$H = H_0 + kd^{-1/2}$$

where H_0 is a material constant and H is the hardness of the material. The Hall-Petch constants k collected by Zhang et al. [62] for several metals are listed in Table 1.2.

Table 1.2: Hall-Petch constants for different metals [62]

Nanometals	fcc-Cu	fcc-Ni	hcp-Mg	bcc-Cr	bcc-Fe	bcc-Mo
k (MPa $\mu m^{1/2}$)	155	695	630	950	980	1650

REFERENCES

[1] Read MH, Altman C. Applied Physics Letters 1965;7:51.

[2] Schwartz N, Reed WA, Polash P, Read MH. Thin Solid Films 1972;14:333.

[3] Grosser M, Schmid U. Thin Solid Films 2009;517:4493.

[4] Gladczuk L, Patel A, Paur CS, Sosnowski M. Thin Solid Films 2004;467:150.

[5] Papp JF. 2010 Minerals Yearbook, Niobium (Columbium) and Tantalum. U.S. Department of the Interior, U.S. Geological Survey; 2012.

[6] Matson DW, Merz MD, McClanahan ED. Journal of Vacuum Science & Technology A: Vacuum, Surfaces, and Films 1992;10:1791.

[7] Catania P, Doyle JP, Cuomo JJ. Journal of Vacuum Science & Technology A: Vacuum, Surfaces, and Films 1992;10:3318.

[8] Moseley PT, Seabrook CJ. Acta Cryst 1972;B29:1170.

[9] Arakcheeva A, Chapuisa G, Grinevitch V. Acta Crystallographica Section B Structural Science 2002;B58:1.

[10] Duckworth RG. Thin Solid Films 1972;10:337.

[11] Iimura Y, Miyashita H, Sana H. Journal of Vacuum Science & Technology B: Microelectronics and Nanometer Structures 1989;7:1680.

[12] Oda M, Ozawa A, Ohki S, Yoshihara H. Japanese Journal of Applied Physics 1990;29:2616.

[13] Sosniak J. Journal of Applied Physics 1967;38:3041.

[14] Westwood WD, Boynton RJ, Wilcox PS. Thin Solid Films 1973;16:1.

[15] Navid a. a., Hodge a. M. Materials Science and Engineering: A 2012;536:49.

[16] Clevenger LA, Mutscheller A, Harper JME, Cabral C, Barmak K. Journal of Applied Physics 1992;72:4918.

[17] Schauer A, Peters W, Bauelemente U. Thin Solid Films 1975;27:95.

[18] Feinstein LG, Huttemann RD. Thin Solid Films 1973;16:129.

[19] Catania P, Roy R a., Cuomo JJ. Journal of Applied Physics 1993;74:1008.

[20] Chen GS, Lee PY, Chen ST. Thin Solid Films 1999;353:264.

[21] Baker PN. Thin Solid Films 1972;14:3.

[22] Knepper R. Thermalmechanical Behavior and Microstructure Evolution of Tantalum Thin Films During the β-α Phase Transformation. Cornell University, 2007.

[23] Lee SL, Doxbeck M, Mueller J, Cipollo M, Cote P. Surface and Coatings Technology 2004;177-178:44.

[24] Arakcheeva A, Chapuis G, Birkedal H, Pattison P, Grinevitch V. Acta Crystallographica Section B Structural Science 2003;B59:324.

[25] Jiang A, Tyson TA, Axe L. Journal of Physics: Condensed Matter 2005;17:6111.

[26] Sato S. Thin Solid Films 1982;94:321.

[27] Zhang J, Huai Y, Chen L, Zhang J. Journal of Vacuum Science & Technology B: Microelectronics and Nanometer Structures 2003;21:237.

[28] Marcus RB, Quigley S. Thin Solid Films 1968;2:467.

[29] Yuan Z, Zhang DH, Li CY, Prasad K, Tan CM, Tang LJ. Thin Solid Films 2003;434:126.

[30] Baker PN. Thin Solid Films 1972;14:3.

[31] Schwartz N, Feit ED. Journal of the Electrochemical Society 1977;124:123.

[32] Westwood WD. Applied Physics Letters 1970;17:264.

[33] Croset M, Velasco G. 1972;1444.

[34] Thornton JA. Journal of Vacuum Science & Technology 1974;11:666.

[35] Navid AA, Hodge AM. Scripta Materialia 2010;63:867.

[36] Thornton, John A., HOFFMAN DW. 1989;171:5.

[37] Detor AJ, Hodge AM, Chason E, Wang Y, Xu H, Conyers M, Nikroo A, Hamza A. Acta Materialia 2009;57:2055.

[38] Mani A, Aubert P, Mercier F, Khodja H, Berthier C, Houdy P. Surface and Coatings Technology 2005;194:190.

[39] Windischmann H. Critical Reviews in Solid State and Materials Sciences 1992;17:547.

[40] Javed A., Sun J-B. Applied Surface Science 2010;257:1211.

[41] Knepper R, Baker SP. Applied Physics Letters 2007;90:181908.

[42] Lee H-J, Kwon K-W, Ryu C, Sinclair R. Acta Materialia 1999;47:3965.

[43] Oliver WC, Pharr GM. J Mater Res 1992;7:1564.

[44] Sneddon IN. International Journal of Engineering Science 1965;3:47.

[45] Kunitake ME, Mangano LM, Peloquin JM, Baker SP, Estroff LA. Acta Biomaterialia 2013;9:5353.

[46] Oliver W. Journal of Materials Research 2004;19:3.

[47] Saha R, Nix WD. Acta Materialia 2002;50:23.

[48] Tsui TY, Vlassak J, Nix WD, Introduction I. Journal of Materials Research 1999;14:2196.

[49] Tsui TY, Vlassak J, Nix WD. Journal of Materials Research 1999;14:2204.

[50] LaFontaine WR, Paszkiet C a., Korhonen M a., Li C-Y. Journal of Materials Research 1991;6:2084.

[51] Hutchings IM. Journal of Materials Research 2009;24:581.

[52] Tsui TY, Oliver WC, Pharr GM. Journal of Materials Research 1996;11:752.

[53] Bolshakov A, Oliver WC, Pharr GM. Journal of Materials Research 1996;11:760.

[54] Ma ZS, Zhou YC, Long, SG, Lu C. Surface and Coatings Technology 2012;207:305.

[55] Lee Y-H, Kwon D. Scripta Materialia 2003;49:459.

[56] Suresh S, Giannakopoulos a. E. Acta Materialia 1998;46:5755.

[57] Carlsson S, Larsson P. Acta Materialia 2001;49:2179.

[58] Carlsson S, Larsson P. Acta Materialia 2001;49:2193.

[59] Ling L, Long S, Ma Z, Liang X. Journal of Materials Science & Technology 2010;26:1001.

[60] Hall EO. Proceedings of the Physical Society 1951;64:747.

[61] Petch NJ. Journal of iron and steel institute 1953;174:25.

[62] Zhang M, Yang B, Chu J, Nieh T. Scripta Materialia 2006;54:1227.

Chapter 2

Experimental details

2.1 Overview

This chapter introduces the experimental techniques used in Chapters 3 and 4. It comprises a brief overview of the film preparation, x-ray diffraction tests and the nanoindentation tests. The work described in section 2.2 and 2.3 was performed by Markus Chmielus and Elizabeth Ellis, both members of the Baker group at Cornell. I performed the work described in section 2.4.

2.2 Film deposition and thermal cycling

Film deposition and thermal cycling were conducted in a custom-made UHV sputter deposition and stress measurement system, shown schematically in Figure 2.1 [1]. The system consists of a high vacuum load-lock chamber and three UHV chambers (with a base pressure lower than 2.7×10^{-6} Pa): a sputter deposition chamber, a transfer chamber and a sample heating chamber for in-situ substrate curvature measurements. Substrates used were Si (100), 100 mm in diameter and 525 μm thick with a native oxide layer. The substrate was placed into the load-lock chamber first and then moved to the sample heating chamber to do the reference substrate curvature measurement. Ta film was subsequently sputtered in the sputter chamber from a 99.95% pure target to a nominal

thickness of 500-600 nm using a magnetron gun operated in DC at 400 W. The key variable was the Ar working gas pressure, p_{Ar}. Seven Ta thin films were prepared at p_{Ar} = 0.3, 0.5, 1.1, 1.6, 1.9, 2.0, and 2.2 Pa (2, 4, 8, 12, 14, 15, and 16 mTorr). To minimize impurities, ultra high purity (UHP) Ar (99.999%) was additionally filtered to further remove oxygen and other contaminants, before being used for both plasma cleaning and deposition. Ta deposition rate was approximately 0.65 ± 0.1 nm/min, independent of p_{Ar} and the substrate temperature increased to a maximum of ~ 90 ℃ during deposition for all samples as measured by a thermocouple on the back side of the substrate. The magnetron sputter guns were oriented 23° from the substrate normal at an average distance of 125 mm. The substrate was rotated at 5 rpm during deposition.

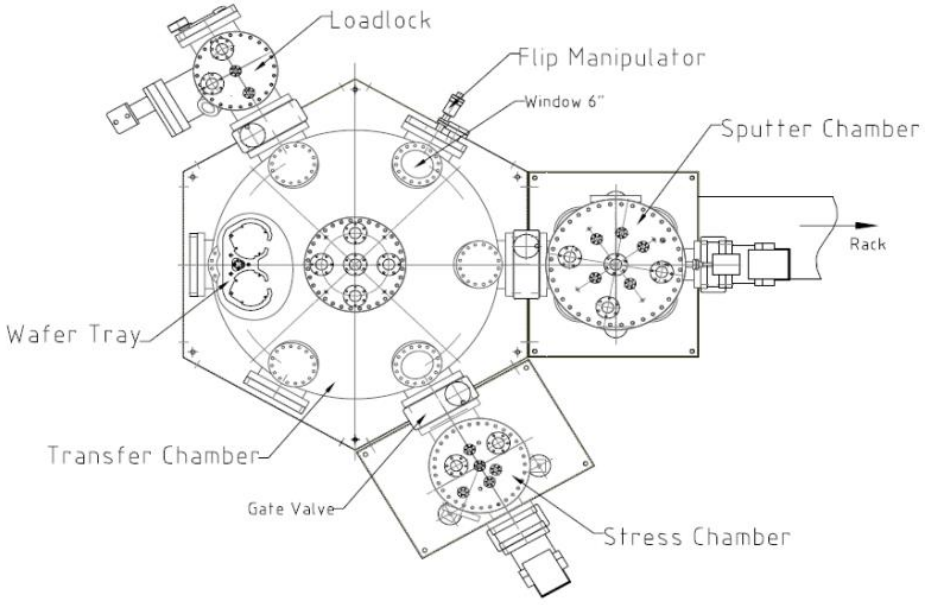

Figure 2.1: Schematic diagram of the UHV system for deposition and thermal cycling [1].

Thermally cycled samples were placed back into the heating chamber after deposition and the stress evolution was measured using a two-dimensional laser scanning method. The biaxial stress was determined by the substrate curvature change:

$$\sigma_f = \frac{Y_s t_s^2}{6t_f}(K - K_0)$$

where K is the curvature after film deposition, K_0 is the initial substrate curvature, t_f is the film thickness, t_s is the substrate thickness and Y_s is the biaxial modulus of the substrate. This equation is commonly known as Stoney equation [2].

2.3 X-ray diffraction

Symmetric x-ray θ-2θ scans were performed to determine the Ta crystal structure present in a given sample. All scans were operated using a Cu k-α source ($\lambda_{\text{Cu-k}\alpha}$: 1.5405 Å) at 40 kV and 44 mA in a continuous scan mode. The scattering vector was 1° off the film normal to avoid the majority of the strong (400) peak from the Si (100) substrate at 2θ = 69.13 °, which is close to the (004) β-Ta (70.89 °) and (211) α-Ta (69.61 °) peaks. Rocking curves of the (002) peak were performed in ω geometry [3] within ±15 ° of the wafer normal for all samples. In-plane texture was investigated with an XRD experiment equipped with a 2D detector. The detector was centered on the (002) β-Ta peak and the sample was rotated around the film normal to 5 random angles between 0 °and 90 °.

2.4 Nanoindentation

A nanoindenter with a Berkovich tip (TI 750, Hysitron Inc., Minneapolis, MN) was used to determine the mechanical properties. Before performing any test on the samples, both the area function of the Berkovich tip and the machine compliance were determined using fused quartz with known hardness (9.25 GPa) and reduced modulus (69.6 GPa). 100 indentations with peak load ranging from 10,000 to 100 uN were made on a quartz sample. The relationship between the total compliance and peak load is given by:

$$C_{total} = \frac{1}{S_{total}} = C_m + \frac{\sqrt{\pi}}{2\beta}\frac{\sqrt{H}}{E_r}\frac{1}{\sqrt{P_{max}}}$$

H and E_r are the hardness and reduced modulus of quartz, C_{total} is the total compliance and C_m is the machine compliance. By linear fitting C_{total} against $\sqrt{P_{max}}$, the intercept given in the fitting, which is the machine compliance, was determined to be C_m = 0.25 nm/mN. In the following indentation tests, the machine compliance was subtracted from the total compliance to yield the contact compliance from the load-depth curves. Then the data were used to derive the area function of the indenter tip. For a Berkovich tip, the projected contact area A has a calibrated relationship with the contact depth h_c:

$$A(h_c) = C_0 h_c^2 + C_1 h_c + C_2 h_c^{1/2} + C_3 h_c^{1/4} + C_4 h_c^{1/8} + C_5 h_c^{1/16}$$

where h_c is the contact depth at maximum load and A is the corresponding projected contact area. The area function works best for contact depths between 40 nm and 110 nm. After determining C_0 through C_5, the model introduced in Chapter 1 can be used to analyze indentation data. Strain rate tests were conducted on the Ta film deposited at 1.1

Pa. Strain rates from 200 to 2,000 μN/s were tried with peak load at 10,000 μN. The results showed no variation of indentation properties with strain rates.

REFERENCES

[1] Knepper R. Thermalmechanical Behavior and Microstructure Evolution of Tantalum Thin Films During the β-α Phase Transformation. Cornell University, 2007.

[2] Stoney GG. Proceedings of the Royal Society of London, Series A 1909;82:172.

[3] McIntyre GJ. Acta Crystallographica Section A 1981;37:105.

Chapter 3

This chapter is a draft of a paper under preparation. My contributions to this work: (1) conducted nanoindentation tests; (2) wrote initial version of discussions on nanoindentation data; (3) participated in discussions on contents and organization of the paper; (4) did literature review of the crystal structure of β-Ta; (5) calculated the mean free path of sputtered Ta atoms.

The influence of sputter gas pressure on the structure and properties of high purity β-tantalum thin films

Markus Chmielus, Elizabeth A. Ellis, Shangchen Han, Shefford P. Baker
Department of Materials Science and Engineering, Cornell University, Bard Hall, Ithaca, NY, USA

3.1 Introduction

Tantalum (Ta) is a very important technological material, especially in microelectronics, which accounts for 70% of the world's Ta consumption [1]. Ta thin films can be deposited in two phases: α- or β-Ta [2–4]. α-Ta is stable, has a bcc crystal structure, and is the only phase present in bulk form. It can be used as capacitors and diffusion barriers between copper and silicon [5–8]. β-Ta is a metastable phase which was found only in thin films, has a high electrical resistivity (~ 180 μΩ cm [9]), and can be etched more easily than α-Ta using reactive ion etching [10]. It is used in thin film resistors, heaters [11–13], and x-ray

optics applications [10,14]. β-Ta has a biaxial modulus of 170 ± 20 GPa [15] and a hardness of 15.02 GPa (with a grain size of 32.3nm) [16]. The crystal structure of β-Ta has long been identified as a σ-type structure belonging to the Frank–Kasper class of tetrahedrally close-packed structure $P4_2/mnm$ [17] space group. In 2002, an improved structure, $P\bar{4}2_1m$ space group [18,19], was proposed to be the right structure. While the former allows only even l for (00l) reflections, the latter allows both even and odd l for (00l) reflections.

Initially, β-Ta was thought to exist only at interfaces or in very thin films smaller than 80 nm [20]. But tests by Matson et al. [21] showed β-Ta in thicker films (up to 130 μm) as well. It was also believed that O or OH needs to be present at the nucleation surface for the formation of β-Ta [2]. This finding was later modified by Sato [22], who observed that substrates with high resistance to oxidation tend to nucleate α-Ta, while substrates with low resistance to oxidation tend to nucleate β-Ta. In a review by Baker [23], it was found that the incorporation of impurities (i.e. Ar, O, H, N) during the sputter process in the Ta thin films might influence the preference for α- or β-Ta. However, results were inconclusive, as with different groups found different phases at higher impurity levels (e.g. Westwood et al. [24] and Read et al. [9]). Croset and Velasco [25], on the other hand, proposed that impurities do not influence the growth of either phase, but that low sputter power and low substrate temperature (also seen in [26]) favor the formation of β-Ta. Baker [23] concluded that while impurities seem to have an influence on which Ta phase is formed, too many parameters change between experimental runs and sputter systems, which also influence

the Ta phase formation. Thus, experiments with controlled changes of parameters are needed.

Many groups have investigated the influence of sputter parameters on sputter-deposited Ta thin film structure and properties including sputter power and substrate temperature [25], substrate bias voltage [27,28], and sputter pressure [28–31] with a large range of base pressures. However, as many studies vary multiple parameters at once or have variations in the sputter environment from sample to sample, it is difficult to separate the effects of each parameter. In this work, we controlled all deposition parameters to ensure constant clean conditions before and during thin film deposition in order to focus solely on the influence of Ar sputter pressure on the structure and properties of Ta thin films.

3.2 Experiments

Ta thin films were sputter deposited onto silicon (Si) substrates in an ultra high vacuum (UHV) deposition system with a base pressure of 2.7×10^{-6} Pa (2.0×10^{-8} Torr) or better. Substrates were (100) Si, 100 mm in diameter and 525 μm thick, with a native oxide layer. Each substrate was plasma cleaned in the deposition chamber for 1 min using a 25 W RF bias at 1.1 Pa Ar. Immediately after cleaning, Ta was sputtered from a 99.95% pure target to a nominal thickness of 500 or 600 nm using a magnetron gun operated in DC at 400 W. The key variable was the Ar working gas pressure, p_{Ar}. Seven Ta thin films were prepared at p_{Ar} = 0.3, 0.5, 1.1, 1.6, 1.9, 2.0, and 2.2 Pa (2, 4, 8, 12, 14, 15, and 16 mTorr). To

minimize impurities, ultra high purity (UHP) Ar (99.999%) was additionally filtered to further remove oxygen and other contaminants, before being used for both plasma cleaning and deposition. The Ta deposition rate was approximately 0.65 ±0.1 nm/min, independent of p_{Ar} and the substrate temperature increased to a maximum of ~ 90 ℃ during deposition for all samples as measured by a thermocouple on the back side of the substrate. The magnetron sputter guns were oriented 23 ºfrom the substrate normal at an average distance of 125 mm. The substrate was grounded and rotated at 5 rpm during deposition. Film stresses were determined by measuring the curvature of the substrates before and after film deposition using a custom curvature measurement system. Curvature measurements were confirmed using a commercial instrument. The Stoney relation [32] was used to determine the stress in each film from the change in curvature.

Following stress measurements, samples were cleaved into pieces of various sizes and shapes for further analyses. High resolution micrographs of the samples' surfaces and cross sections were produced using scanning electron microscopy (SEM). Sample thicknesses were obtained from the cross-section images. For samples produced with p_{Ar} = 0.3, 0.5, and 1.1 Pa, thicknesses were also determined using Rutherford backscattered diffraction (RBS) and the RUMP analysis and simulation software.

The crystal structure present in the Ta films was evaluated using x-ray diffraction (XRD). θ-2θ scans were completed using a Cu k-α (λ=1.5405 Å) source operated at 40 kV and 44 mA. The scattering vector was 1 ºoff the film normal to avoid the majority of the strong (400) peak from the Si (100) substrate at 2θ = 69.13 º, which is close to the (004)

β-Ta (70.89 º) and (211) α-Ta (69.61 º) peaks. Rocking curves of the (002) peak were performed in the ω geometry [33] within ±15 ºof the wafer normal for all samples. In-plane texture was investigated by an XRD experiment equipped with a 2D detector. The detector was centered around the (002) β-Ta peak and the sample was rotated around the film normal to 5 random angles. All x-ray measurements were performed on a piece from the center of the substrate for all samples.

A scanning nanoindenter with a Berkovich tip (TI 750, Hysitron Inc., Minneapolis, MN) was used to determine the mechanical properties of the films. 64 indentations with peak load from 1,000uN to 10,000uN were made in each film. The hardness and reduced modulus values were extracted from the load-depth data using the Oliver & Pharr method [34]. Reduced modulus was then converted into indentation modulus $E/(1-\nu^2)$ to represent the sample specific modulus [35], where E and ν are Young's modulus and Poisson's ratio of the material respectively. The indenter can also serves as an imaging probe to obtain the surface topography. Indentations with indentation depth of 160 nm on the films deposited at 0.3 and 2.2 Pa Ar pressure were scanned to detect the indentation morphology.

3.3 Results

XRD measurements (Figure 3.1 (a)) revealed that all films are β-Ta and have good (002) texture. Magnifying by 50× (Figure 3.1 (b)) reveals nearly negligible (410), (202), and (212) β-Ta peaks. A small peak at 2θ = 52.5 ºwas identified as (003) β-Ta as in Jiang et al. [36], not as (200) α-Ta (~ 55.5 º, too far away) or (521) β-Ta (~51.1 º, but intensity factor is

very small). The height of the (002) and (004) β-Ta peaks decreased continuously with increasing sputter pressure by nearly a factor of 40 while the 2θ peak width remained constant. Rocking curves of the (002) β-Ta peak (Figure 3.2 inset) increased in breadth from 6 ºto 24 ºacross the pressure range. The breadths of the rocking curves for the 2.0 and 2.2 Pa samples are underestimated due to constraints of the ω geometry used in the rocking curve scans. Texture scans made in the plane of the films showed random in-plane orientation distributions.

SEM micrographs of as-deposited Ta thin films displayed different surface feature characteristics as a function of p_{Ar} (Figure 3.3). Samples deposited at 0.3, 0.5, and 1.1 Pa had small worm-like surface features. With increasing sputter pressure, the surface features increase in size and began to appear pyramidal in shape. The average grain size was determined by the average distance between the local maxima of grey values along four line profiles (vertical, horizontal, ± 45 º) on each micrograph (each line had between 20 and 60 local maxima). The change in grain size is summarized in Figure 3.4. While the 0.3 Pa sample had an average grain size of 24 nm, the grain size increased to an average of 81 nm for the sample deposited at 2.2 Pa. The cross section micrograph (inset in the 1.6 Pa micrograph) shows cleaved edge of the film, where brittle fracture reveals a fine-grained columnar structure.

Equal biaxial in-plane stresses also varied with Ar sputter pressure. As shown in Figure 3.5, stresses determined from substrate curvature increased continuously with increasing sputter pressure from -1,360 MPa to 1,140 MPa across the pressure range. The

change in stress was also visible in a continuous shift of the (002) β-Ta XRD peak positions (Figure 3.5 inset) towards higher 2θ, from 33.634 ° to 34.116 ° across the pressure range. Calculating the change in strain, $\Delta\varepsilon_z$, in the film normal direction from this 2θ shift, and calculating the corresponding change in in-plane film stress $\Delta\sigma_f$ from $\Delta\sigma_f = Y((1-\nu)/2\nu)\Delta\varepsilon_z$, where $Y = 170 \pm 20$ GPa [15] is the biaxial modulus and using $\nu = 0.3$ as the Poisson ratio, we get $\Delta\sigma_f = 2.72$ GPa, in agreement with the stresses determined from substrate curvature.

Figure 3.6 shows the indentation modulus and hardness values vs. contact depth for the film deposited at 0.3 Pa Ar pressure. For the indentations with contact depth larger than 40 nm, the hardness decreased from ~ 16.4 GPa to ~ 15.7 GPa and the indentation modulus decreased from ~ 212 GPa to ~ 199 GPa.

3.4 Discussion

3.4.1 Structure characterization

3.4.1.1 Phase identification and β-Ta structure

The preferred phase in as-deposited Ta films has been studied before but the results are always confusing. The films studied here showed only β-Ta phase over the entire Ar pressure range, in contrast to results published by Navid et al. [37] who got α-Ta at Ar pressures of 0.5 and 0.7 Pa. The consistent presence of only β-Ta phase indicated a good control over the sputter parameters in the present study.

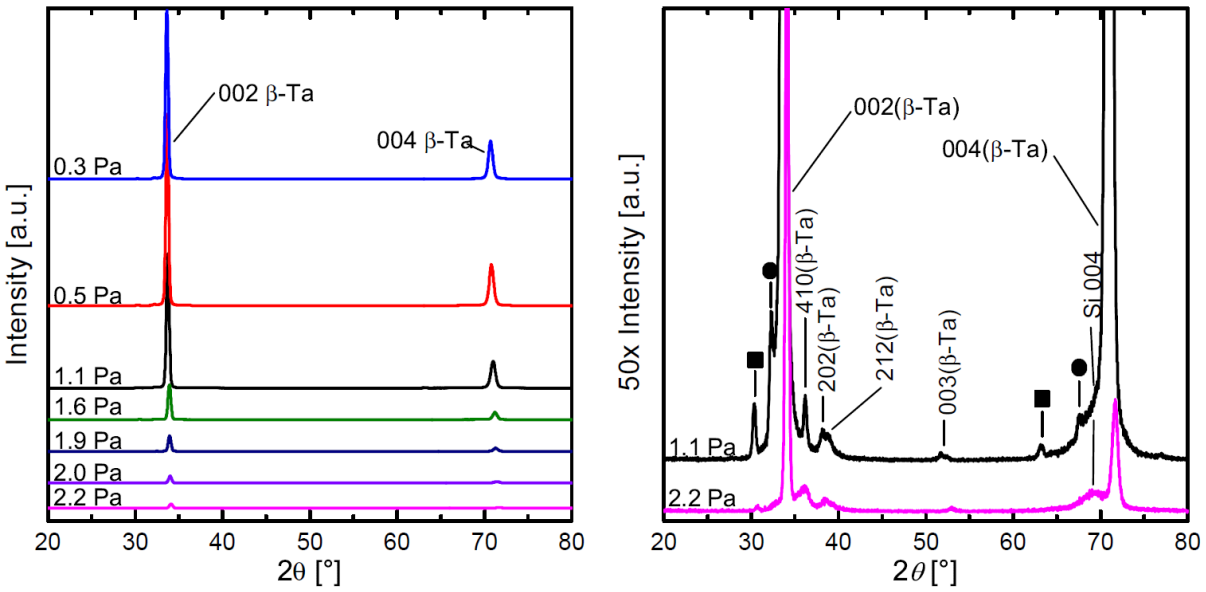

Figure 3.1: X-ray diffraction (Cu K-α) θ-2θ scans of as-deposited Ta thin films as a function of Ar sputter gas pressure. The inset shows details of smaller peaks by magnifying intensity by a factor of 50. Black squares indicate reflections caused by Cu K-β radiation and black circles by W L-α radiation. All films are β-Ta with very good (002) fiber texture.

Although the early proposed $P4_2/mnm$ [17] structure for β-Ta in 1972 was widely accepted, the improved $P\bar{4}2_1m$ structure proposed by Arakcheeva et al. [18] in 2002 has also been supported [38,39] by the identification of odd (00*l*) diffractions. The diffraction peaks between the (002) and (004) peaks range from 51.4 °at 0.3 Pa to 52.5 °at 2.2 Pa. The nominal (003) peak position is at 51.6 ° (Figure 3.1). As the angular deviation from the nominal peak position is approximately halfway between the deviation of the (002) and (004) peaks, and therefore appears to depend on film stresses, this peak can be identified with a high degree of certainty as the (003) β-Ta. The appearance of this peak strongly

indicates that $P\bar{4}2_1m$ structure is the correct structure for β-Ta.

3.4.1.2 Rocking curve scans and texture

To the authors' knowledge, there are no rocking curves reported for Ta thin films so far, which are on the other hand very common in other materials, where highly textured films are of great importance (e.g. in AlN thin films [40] rocking curve FWHM increases slightly with increasing sputter pressure). The increase in rocking curve FWHM (Figure 3.2) with increasing sputter pressure can be attributed to an increase in the frequency of collisions between sputter gas atoms and Ta atoms. Ta atoms sputtered in lower-pressure environments are not expected to go through high frequency of collisions. On the other hand, Ta atoms sputtered in higher-pressure environments are more likely to experience collisions before reaching the substrate. Increased collision rates cause a decrease in adatom mobility [41] and adatoms will thus be less able to reach an equilibrium site. Adatoms are also expected to approach the substrate at oblique angles [42] when the frequency of collisions is high. This leads to a broad distribution of nucleus orientations. Combination of change in both adatom mobility and angle distribution of incoming sputtered Ta atoms with Ar pressure can account for the observed increase in rocking curve FWHM.

The measured β-Ta (002) peak heights in this study decreased by a factor of 40 as Ar pressure increased while other texture components did not increase in intensity. Many researchers have reported some degree of (002) texture in as-deposited β-Ta thin films. In

the review by Baker [23] about Ta thin films, the out-of-plane peak intensity mostly seemed to decrease with increasing sputter pressure. In this study, even though the (002) peak height decreases with increasing sputter pressure, no other peak appears or increases, indicating (002) texture even at high sputter pressure. The peak height decrease agrees with the rocking curve broadening since the (002) texture component has a wider distribution with increasing Ar pressure.

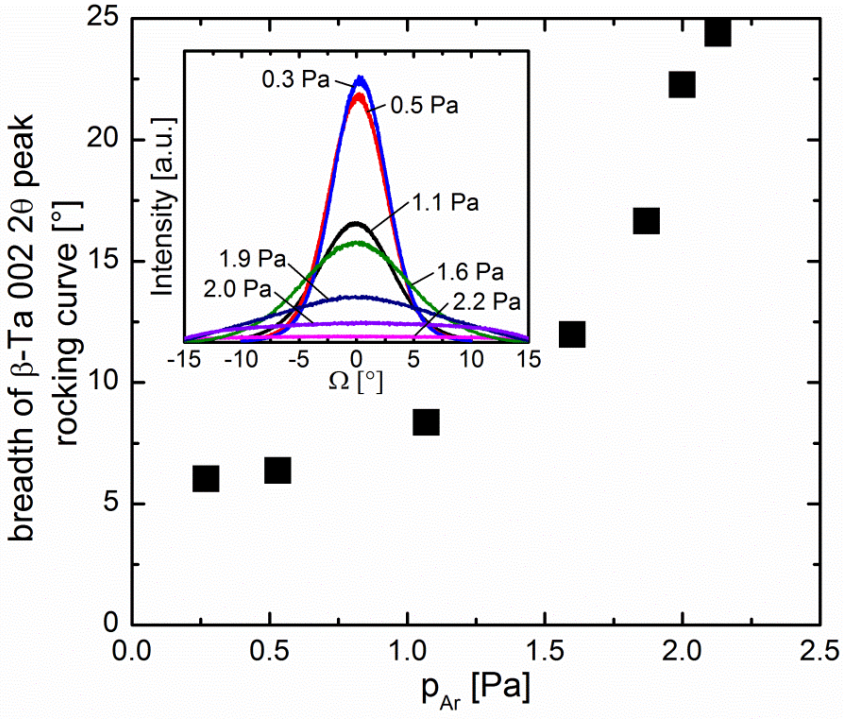

Figure 3.2: Breadth (FWHM) of x-ray diffraction rocking curves from Ta films as a function of Ar sputter gas pressure (inset shows rocking curves). Due to the geometry of the scan, the actual breadths of orientation distributions for films sputtered at 2.0 and 2.2 Pa are most likely larger than indicated.

3.4.1.3 Grain size

Grain size increased from 24 nm to 81 nm with increasing sputter pressure from 0.3 to 2.2 Pa, while the out-of-plane grain size did not, according to a Scherrer analysis of the (002) Ta peak FWHM. The increase of grain size has also been found by Grachev et al. [43]. TEM cross sections of Cr thin films indicated an increase in the average grain width from 50 to 100 nm with increasing Ar sputter pressure from 0.5 to 2.2 Pa. Similarly, the surface feature diameter of their Cr films increased in a similar fashion and the grains were columnar and extended through the entire film thickness.

3.4.1.4 Stress variations

While the transition from compressive to tensile stress occurs at a different Ar pressure than in other experiments (e.g. ~ 1 Pa [30], ~ 2 Pa [44], ~ 14 Pa [28]), the transition is always consistent from compressive to tensile. This effect is explained by the changing energy of Ta atoms and reflected Ar neutrals arriving at the sputtered film with changing sputter pressure. Mani et al. [45] predicted that the atoms will reach the substrate without collisions when the mean free path of sputtered atoms is equal to or larger than the target–substrate distance. Otherwise, Ta atoms have collisions with Ar atoms before reaching the substrate and their energy decreases. The mean free path calculated from the following equation is given for our pressure range [46] in Table 3.1:

$$\lambda = \frac{kT}{\sqrt{2}\pi d^2 p} \qquad (1)$$

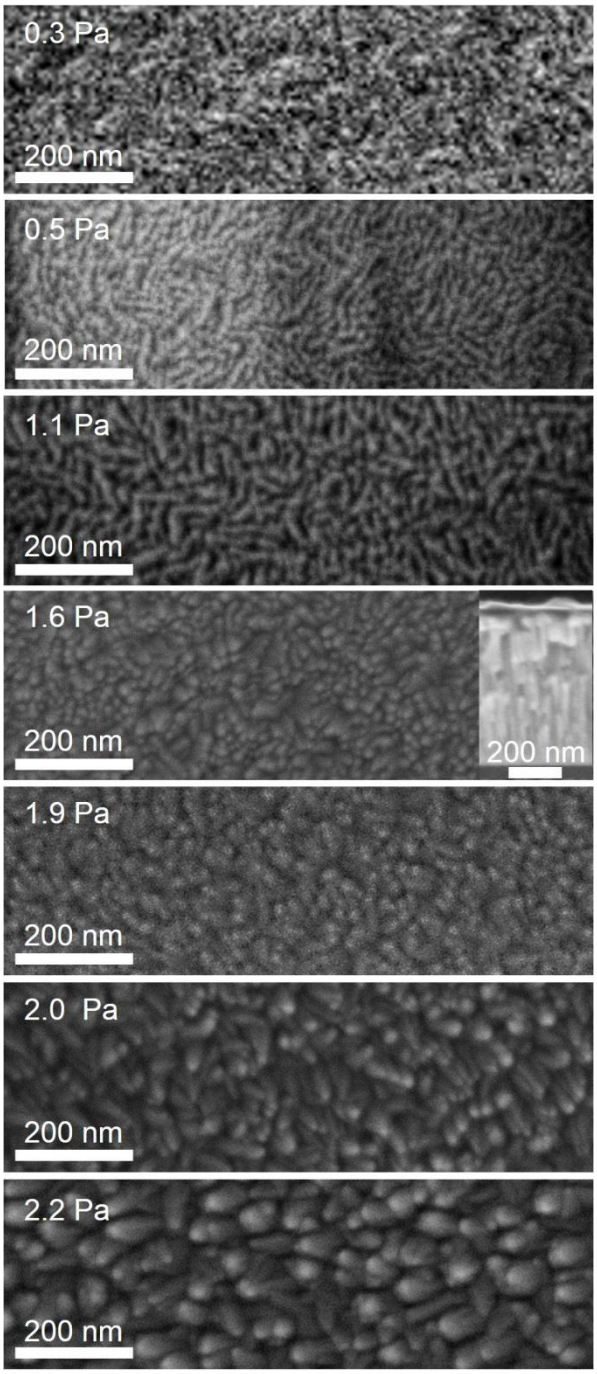

Figure 3.3: Micrographs of the surfaces of as-deposited Ta thin films deposited at different Ar gas pressures. Surface features become larger with p_{Ar}. The inset at p_{Ar} = 1.6 Pa shows a representative cross section indicating that the grain structure of the film is columnar.

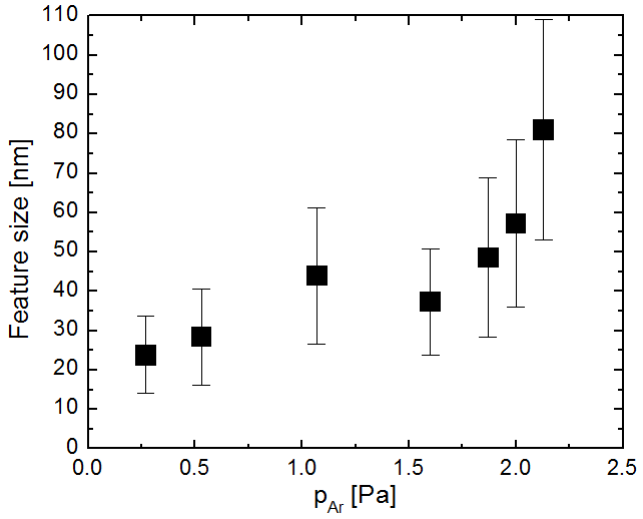

Figure 3.4: Average grain sizes measured from micrographs in Figure 3.3 as a function of Ar sputter pressure.

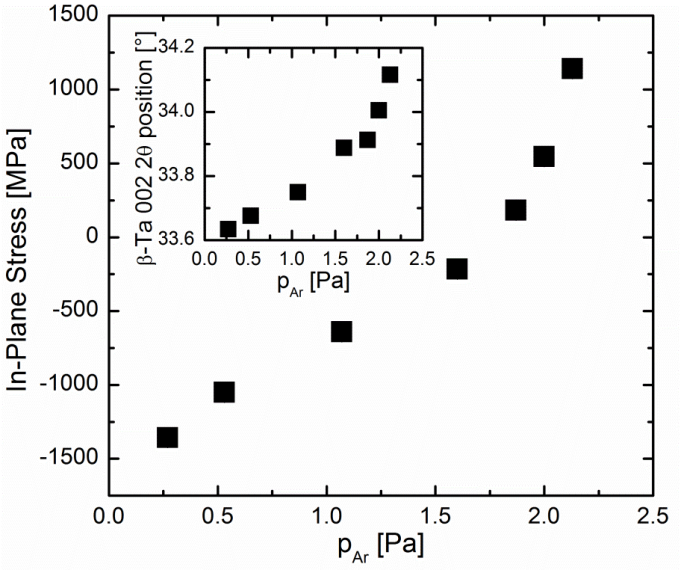

Figure 3.5: Stresses in as-deposited Ta-films as a function of Ar gas pressure determined from substrate curvature. The inset shows the shift of the (002) β-Ta XRD peak position with Ar gas pressure. Stresses go from strongly compressive to strongly tensile over the pressure range.

where k is the Boltzmann constant (1.38×10^{-23}), T is the temperature (298 K), d is the diameter of the Ta atom (0.292 nm), p is the Ar pressure.

Since the mean free path for the entire sputter range (Table 3.1) is below the target-wafer distance, collisions always take place. With increasing sputter pressure, the energy of arriving atoms at the thin film consequently decreases. At high energies of incoming species, atomic peening causes compressive stresses (at low pressure) which transitions to grain boundary zipping at high sputter pressure [47].

Table 3.1: Mean free path for films deposited at different Ar gas pressures

p_{Ar}		T	d	λ
[Pa]	[mTorr]	[K]	[cm]	[cm]
0.27	2	298	2.92×10^{-8}	4.08
0.53	4	298	2.92×10^{-8}	2.04
1.07	8	298	2.92×10^{-8}	1.02
1.60	12	298	2.92×10^{-8}	0.68
1.87	14	298	2.92×10^{-8}	0.58
2.00	15	298	2.92×10^{-8}	0.54
2.13	16	298	2.92×10^{-8}	0.51

3.4.2 Hardness and modulus

The hardness and indentation modulus as a function of contact depth for the film deposited at 0.3 Pa Ar pressure were shown in Figure 3.6. The indentation data below 40 nm were not considered in analysis due to the tip rounding effect. The observation that the substrate has a more significant effect on indentation modulus than on hardness is

expected since hardness is mostly related to the localized plastic deformation while the indentation modulus is related to the elastic deformation around the indentation area, which could extend to a much wider region. To avoid the substrate effect and the tip rounding effect, indentations with contact depths between 40 nm and 60 nm (~ 10 indentations) were averaged for all the films to study the indentation properties of the films (Figure 3.7).

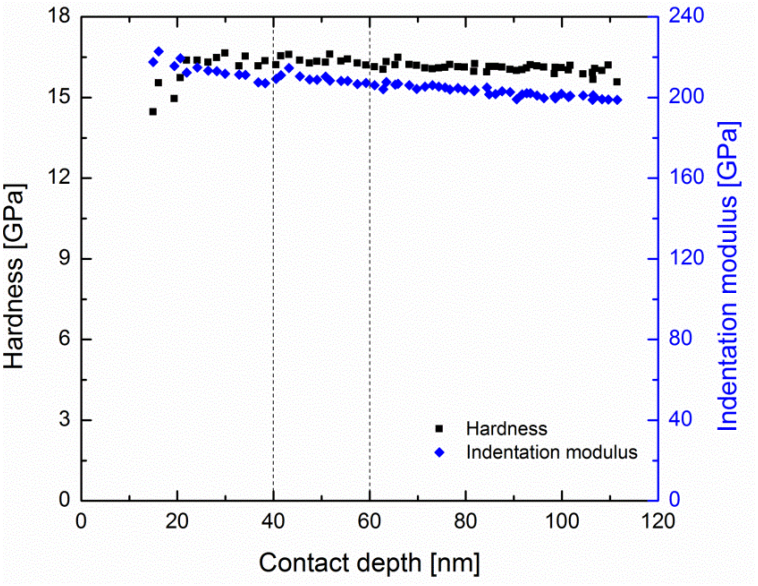

Figure 3.6 Hardness and indentation modulus as a function of contact depth for the film deposited at 0.3 Pa. Contact depths between 40 nm and 60 nm were averaged to represent the film properties (Figure 3.7).

Tsui [48] and Bolshakov [49] pointed out that different stress levels can affect the measured hardness and modulus. The reason was indentation pile-up which results in a wrong estimation of the contact area. In other words, the existence of residual stress

could invalidate the nanoindentation model [34] due to introduction of pile-up. Scans of indentations with depth of 160 nm on both the 0.3 Pa and 2.2 Pa films showed that maximum pile-up height around an indentation for the low pressure film is ~ 8 nm while the maximum pile-up height around an indentation for the high pressure film is ~ 9 nm. It was also pointed out by Oliver and Pharr [50] that pile-up is small when $h_f/h_{max} < 0.7$ (h_f is the residual indentation depth, h_{max} is the depth at maximum load) whereas in our case, this ratio is ~ 0.5. Considering that the stress difference between the two films is as high as ~ 2.5 GPa, it is concluded here that stress has a very small influence on indentation pile-up in β-Ta and thus the indentation results are valid for further analysis.

The constant indentation modulus (Figure 3.7) indicates a nearly constant density of the β-Ta films over the entire Ar pressure range, with the exception of the highest sputter pressure (2.2 Pa) film, where the density of the film might be lower. The density reduction could be caused by grain boundaries not being able to zip together anymore and therefore a porosity increase [47]. The Young's modulus reported by Zhang et al. [51] for nanocrystalline β-Ta is 193.87 GPa. If we assume they used a Poisson ratio of 0.3 in analysis, the calculated indentation modulus was ~ 213.04 GPa which is very close to our low pressure films.

Tsui [48] and Bolshakov's [49] studies of the effect of stress on nanoindentation tests by experiments and finite element analysis respectively showed that the real hardness is not affected by stress which has been the basis of several numerical models [52–55]. Carlsson and Larsson [54,55] studied effects of residual elastic stress and plastic

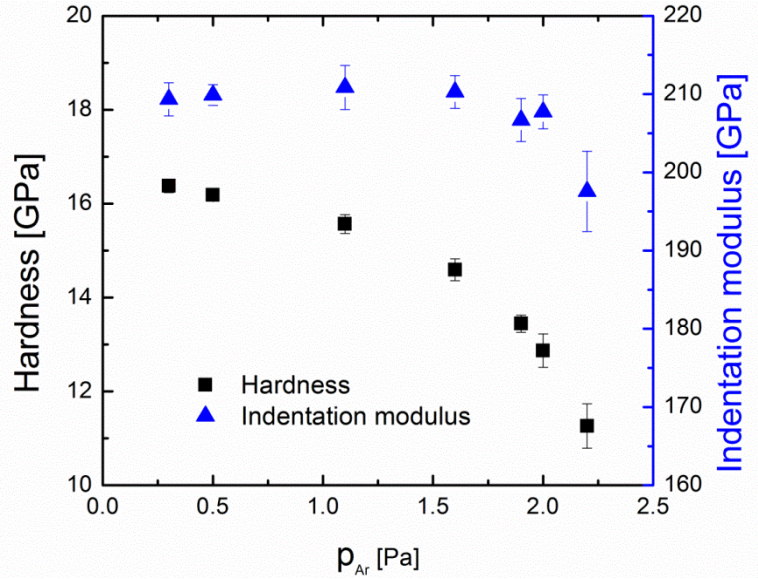

Figure 3.6: Indentation modulus and hardness of as-deposited Ta films as a function of Ar sputter gas pressure. The modulus is insensitive to p_{Ar} except for the highest-pressure film, while the hardness decreases with p_{Ar}.

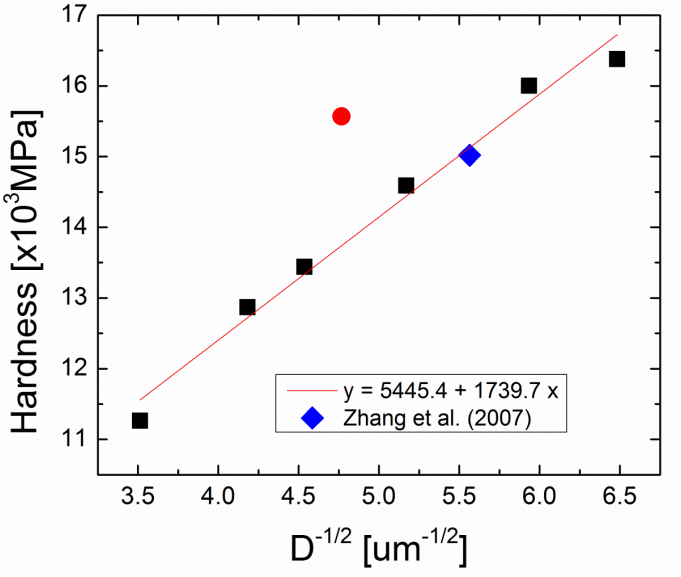

Figure 3.7: Linear fitting of the hardness vs. $D^{-1/2}$ of Ta films. The circle is a data point (film deposited at 1.1 Pa Ar pressure) deviating from the Hall-Petch relationship and was not included in the fitting. The diamond in the plot is the data from Zhang et al. [16].

strain on indentation data and concluded that elastic stress only affects the indentation pile-up while plastic strain increases the yield stress of the material and enhance the hardness of the material. Similar conclusion was also made by Ling et al. [56]. In our study, pile-up is too small to affect indentation data and the effect of elastic stress on hardness can be excluded. It is also reasonable to conclude little or no plastic strain in these films based on the monotonous hardness decrease with increasing film stress.

On the other hand, how the grain size affects the hardness has long been recognized as the Hall-Petch relationship:

$$H(D) = H_\infty + k_H D^{-1/2} \quad (2)$$

where $H(D)$ is the grain size dependent hardness, H_∞ is the hardness of the coarse-grained β-Ta and k_H is the Hall-Petch constant, the slope of the $H(D)$ vs. $D^{-1/2}$ plot. A Hall-Petch correlation is plotted as shown in Figure 3.7. Except for the 1.1 Pa sample, all the films followed a good linear relationship in this plot. Zhang et al. [16] deposited β-Ta with base pressure of 1.07×10^{-5} Pa and sputter pressure of 0.67 Pa and got a β-Ta film with grain size of 32.3 nm and hardness of 15.02 GPa. Their data is marked by a diamond in Figure 3.7 and fits for our Hall-Petch plot. The Hall-Petch constant for β-Ta was determined to be 1739.7 MPa $\mu m^{1/2}$. This value is higher than all that of the bcc, fcc and hcp metals summarized by Zhang et al. [51] where Mo (bcc structure) has the highest Hall-Petch constant (1650 MPa $\mu m^{1/2}$). This means that the complex four layer stacking structure of β-Ta makes dislocation more difficult to slip than the bcc, fcc and hcp systems [16]. Hardness extracted for coarse grained β-Ta was determined to be 5.45 GPa.

REFERENCES

[1] Papp JF. 2010 Minerals Yearbook, Niobium (Columbium) and Tantalum. U.S. Department of the Interior, U.S. Geological Survey; 2012.

[2] Feinstein LG, Huttemann RD. Thin Solid Films 1973;16:129.

[3] Catania P, Roy R a., Cuomo JJ. Journal of Applied Physics 1993;74:1008.

[4] Ino K. Journal of Vacuum Science & Technology A: Vacuum, Surfaces, and Films 1997;15:2627.

[5] Holloway K, Fryer PM. Applied Physics Letters 1990;57:1736.

[6] Clevenger LA, Bojarczuk NA, Holloway K, Harper JME, Cabral C, Schad RG, Cardone F, Stolt L. Journal of Applied Physics 1993;73:300.

[7] Laurila T, Zeng K, Kivilahti J, Molarius J, Suni I. Journal of Materials Research 2001;16:2939.

[8] Burgess S. Microelectronic Engineering 2002;64:307.

[9] Read MH, Altman C. Applied Physics Letters 1965;7:51.

[10] Kondo K, Nakabayashi M, Kawakami K, Chijimatsu T, Nakaishi M, Yamada M, Yamabe M, Sugishima K. Journal of Vacuum Science & Technology A: Vacuum, Surfaces, and Films 1993;11:3067.

[11] Westwood W, Livermore F. Thin Solid Films 1970;5:407.

[12] Baker PN. Thin Solid Films 1970;6:R57.

[13] Schwartz N, Reed WA, Polash P, Read MH. Thin Solid Films 1972;14:333.

[14] Yoshihara T, Suzuki K. Journal of Vacuum Science & Technology B: Microelectronics and Nanometer Structures 1994;12:4001.

[15] Knepper R, Baker SP. Applied Physics Letters 2007;90:181908.

[16] Zhang M, Zhang YF, Rack PD, Miller MK, Nieh TG. Scripta Materialia 2007;57:1032.

[17] Moseley PT, Seabrook CJ. Acta Cryst 1972;B29:1170.

[18] Arakcheeva A, Chapuisa G, Grinevitch V. Acta Crystallographica Section B Structural Science 2002;B58:1.

[19] Arakcheeva A, Chapuis G, Birkedal H, Pattison P, Grinevitch V. Acta Crystallographica Section B Structural Science 2003;B59:324.

[20] Schauer A, Peters W, Bauelemente U. Thin Solid Films 1975;27:95.

[21] Matson DW, Mcclanahan ED, Lee SL, Windover D. Surface and Coatings Technology 2001;146-147:344.

[22] Sato S. Thin Solid Films 1982;94:321.

[23] Baker PN. Thin Solid Films 1972;14:3.

[24] Westwood WD, Waterhouse N. Journal of Applied Physics 1971;42:2946.

[25] Croset M, Velasco G. Journal of Applied Physics 1972;43:1444.

[26] Schauer A, Roschy M, Bauelemente U. Thin Solid Films 1972;12:313.

[27] Ren H, Sosnowski M. Thin Solid Films 2008;516:1898.

[28] Clevenger LA, Mutscheller A, Harper JME, Cabral C, Barmak K. Journal of Applied Physics 1992;72:4918.

[29] Grosser M, Schmid U. Thin Solid Films 2009;517:4493.

[30] Navid AA, Hodge AM. Scripta Materialia 2010;63:867.

[31] Javed A., Sun J-B. Applied Surface Science 2010;257:1211.

[32] Stoney GG. Proceedings of the Royal Society of London, Series A 1909;82:172.

[33] McIntyre GJ. Acta Crystallographica Section A 1981;37:105.

[34] Oliver WC, Pharr GM. J Mater Res 1992;7:1564.

[35] Kunitake ME, Mangano LM, Peloquin JM, Baker SP, Estroff LA. Acta Biomaterialia 2013;9:5353.

[36] Jiang A, Tyson TA, Axe L, Gladczuk L, Sosnowski M, Cote P. Thin Solid Films 2005;479:166.

[37] Navid AA, Hodge AM. Materials Science and Engineering: A 2012;536:49.

[38] Jiang A, Tyson T a., Axe L, Gladczuk L, Sosnowski M, Cote P. Thin Solid Films 2005;479:166.

[39] Lee SL, Doxbeck M, Mueller J, Cipollo M, Cote P. Surface and Coatings Technology 2004;177-178:44.

[40] Iriarte GF, Rodriguez JG, Calle F. Microsystem Technologies 2011;17:381.

[41] Thornton JA. Annual Review of Materials Science 1977;7:239.

[42] Thornton JA. Journal of Vacuum Science & Technology A: Vacuum, Surfaces, and Films 1985;3:576.

[43] Grachev SY, Tichelaar FD, Janssen GC a. M. Journal of Applied Physics 2005;97:073508.

[44] Thornton JA, Hoffman DW. Journal of Vacuum Science & Technology 1977;14:164.

[45] Mani A, Aubert P, Mercier F, Khodja H, Berthier C, Houdy P. Surface and Coatings Technology 2005;194:190.

[46] Detor AJ, Hodge AM, Chason E, Wang Y, Xu H, Conyers M, Nikroo A, Hamza A. Acta Materialia 2009;57:2055.

[47] Windischmann H. Critical Reviews in Solid State and Materials Sciences 1992;17:547.

[48] Tsui TY, Oliver WC, Pharr GM. Journal of Materials Research 1996;11:752.

[49] Bolshakov A, Oliver WC, Pharr GM. Journal of Materials Research 1996;11:760.

[50] Oliver W. Journal of Materials Research 2004;19:3.

[51] Zhang M, Yang B, Chu J, Nieh T. Scripta Materialia 2006;54:1227.

[52] Lee Y-H, Kwon D. Scripta Materialia 2003;49:459.

[53] Suresh S, Giannakopoulos a. E. Acta Materialia 1998;46:5755.

[54] Carlsson S, Larsson P. Acta Materialia 2001;49:2179.

[55] Carlsson S, Larsson P. Acta Materialia 2001;49:2193.

[56] Ling L, Long S, Ma Z, Liang X. Journal of Materials Science & Technology 2010;26:1001.

Chapter 4

Hardness and modulus of phase transformed α-Ta thin films

The β-Ta films described in Chapter 3 (deposited at Ar pressure from 0.3 to 2.2 Pa) were thermally cycled to 700 ℃. All the films followed a thermoelastic behavior at first and then the stress jumped at ~ 350 ℃ corresponding to the expected phase transformation from β-Ta to α-Ta. After the phase transformation, α-Ta films followed a thermoelastic behavior again. All phase transformed α-Ta films ended up at the same stress, indicating the densification model previously proposed [1] is insufficient in explaining the phase transformation. A structure with orientation gradient and discontinuous grain boundaries was identified for each film from the EBSD mappings. Contrary to the strongly textured as-deposited β-Ta films, all phase transformed α-Ta films show a continuous orientation gradient structure [1]. The gradient structure was proposed to be accommodated by aligned arrays of edge dislocations on primary slip systems parallel or nearly parallel to the plane of the film. The orientation gradient decreases from ~ 22º/μm to ~ 10º/μm with increasing Ar pressure indicating a decrease in dislocation density with increasing Ar pressure. In the EBSD mappings, areas with misorientation greater than 8 ºwere defined as grain boundaries in analyses and used to determine the boundary spacing. It was determined that average boundary spacing of the α-Ta films is always bigger than 1 μm and increases with Ar pressure.

64 indentations with 10 μm spacing away from each other were made on each film at an indentation load of 1,000 μN. It is seen that indentation modulus (Figure 4.1) decreases with increasing Ar pressure from 187 GPa to 171 GPa. The hardness variation with Ar pressure also follows a decreasing trend (from 4.0 GPa to 3.1 GPa) except for the film deposited at 1.6 Pa Ar pressure. The contact depths are generally around 60 nm indicating length of the edge of residual indentation is ~ 450 nm. It seems that although the boundary spacing is changing in these films, it is always larger than the indentation size and thus grain boundaries should have a small effect on the measured hardness. However, our films obviously have higher hardness (between 3 and 4 GPa) than that of coarse-grained bulk α-Ta (1.17 GPa) [2]. Grain boundaries < 8 °should still be acting to block dislocation motions and results in the decrease in hardness with Ar pressure. Also, the pre-existing dislocations can also strengthen hardness. As Dub et al. pointed out [3] that during the indentation process, the pre-existing dislocations can interact with the dislocation loops created during the indentation process. In our study, pre-existing dislocations block the dislocation motion and enhance the hardness of the films. Lower dislocation densities in higher pressure films are also responsible for their lower hardness.

Young's modulus calculated for each orientation based on the elastic constants [4] of α-Ta are: $E_{<100>}$=142.4 GPa, $E_{<110>}$=190.7 GPa, $E_{<111>}$=214.9 GPa. It can be seen that <111> is a stiffer orientation and <100> is a more compliant orientation. We can infer that the low pressure film has a lower composition of <100> and therefore a higher modulus

while the high pressure film has a higher composition of <100> and therefore a lower modulus.

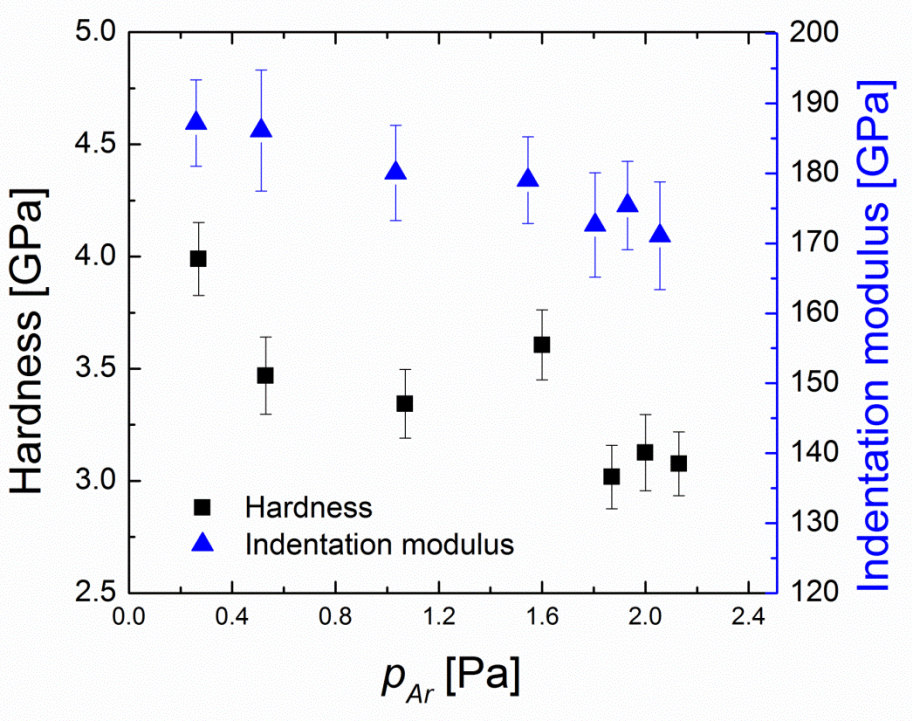

Figure 4.1: Hardness and indentation modulus of phase transformed α-Ta films as a function of Ar pressure.

Zhang et al. [2] studied the nanoindentation properties of an α-Ta film with an average grain size of 76.5 nm. According to their XRD θ-2θ result, the film has a strong (110) texture. Hardness and Young's modulus reported are 11.6 GPa and 178 GPa respectively for their nanocrystalline α-Ta. If we assume they used a Poisson ratio of 0.3 in analysis, the indentation modulus was 195.6 GPa. Their nanocrystalline α-Ta apparently has a much higher hardness than the phase transformed α-Ta indicating that

grain boundaries with large spacing in phase transformed α-Ta are not as effective in blocking dislocation motions. The lower moduli of phase transformed α-Ta than that of their strong (110) textured α-Ta can be attributed to the presence of compliant <100> out-of-plane orientation components in the phase transformed α-Ta.

REFERENCES

[1] Knepper R. Thermalmechanical Behavior and Microstructure Evolution of Tantalum Thin Films During the β-α Phase Transformation. Cornell University, 2007.

[2] Zhang M, Yang B, Chu J, Nieh T. Scripta Materialia 2006;54:1227.

[3] Dub SN, Lim YY, Chaudhri MM. Journal of Applied Physics 2010;107:043510.

[4] Featherston FH, Neighbors JR. Physical Review 1963;130:1324.

Chapter 5

Summary and outlook

Ultrahigh purity Ta films have been deposited with good control of sputter parameters. The films deposited under different Ar pressures showed consistent variations both in structure and indentation properties. All the as-deposited Ta films exhibited a strong (002) β-Ta texture, broadening of rocking curves, increase in grain size, increase in stress, decrease in hardness, constant indentation modulus except for the highest pressure sample with increasing Ar pressure. The hardness decrease can be correlated with the grain size change by the Hall-Petch relationship. As-deposited β-Ta films were thermally cycled to 700 ℃ and a phase transformation from β-Ta to α-Ta occurred. All the films ended up at the same stress after thermal cycling. Decrease in hardness and indentation modulus were both observed with increasing Ar pressure and can be correlated with the dislocation density, grain boundary spacing and components of different orientations in phase transformed α-Ta films.

Further experiments are needed to study the structures and indentation properties of α-Ta films:

(1) TEM — as pointed out in Chapter 4, the orientation gradient structure can be accommodated with aligned dislocations. TEM plan view can be used to analyze dislocation and grain structures in phase transformed α-Ta films to understand

nanoindentation results.

(2) EBSD of indentations — correlating each indentation data with the orientation of the indented region in each film can help understand anisotropy effects in phase transformed α-Ta films in more detail.